

Petrography and Geochemistry framework of the Harzburgite xenoliths of Lake Guinnadji and Ngao Djalsoka volcano from the Dibi area (Adamawa plateau - Cameroon)

Abstract

Petrographic and geochemical studies have been carried out on the peridotite xenoliths included in the pyroclastite deposits from the Lake Guinnadji and Ngao Djalsoka volcano close to the Dibi locality in the Adamawa plateau, central Cameroon. Petrography study reveals The peridotite xenoliths exhibit protogranular and porphyroclastic textures, and are composed of olivine, orthopyroxene and minor amount of clinopyroxene, amphibole (?) and spinel, typical of harzburgite type. ICP-MS and ICP-OES analyses of representative samples show that they are in the range of those of the primitive mantle origin (42.4-45.0 wt.% MgO, 65.7-79.0 wt.% normative olivine). Decreasing SiO₂, TiO₂, Al₂O₃ and CaO contents vs increasing MgO trends evidence depletion from more fertile mantle by extraction of basaltic melts, leaving a refractory residue of harzburgite composition. High contents of REE and incompatible elements point out secondary enrichment processes which have affected the peridotite xenoliths. For this, metasomatism caused by silicate fluids phase could be is invoked. In that way, peridotites of Dibi area witness of the nature and the evolution of lithospheric mantle under the Adamawa plateau.

Keywords: Mantle xenolith, Harzburgite, Melt extraction, Metasomatism, Adamawa plateau, Cameroon

1. Introduction

The basement of African continent is composed of the Archean cratons and Pan African mobile belts (Figure 1A). The Cameroon volcanic line and Adamawa plateau (Figure 1B) are among the main volcanic structures located within the Pan African belt. The studied area (Figure 1C) belongs to the central Adamawa plateau that is an asymmetrical horst of mean altitude of 1100 m with 1 km difference in height vis-à-vis to its vicinity. The horst shape structure of Adamawa took place at during the Tertiary times after its uplift due to the reworking of Pan African faults (Moreau et al., 1987) which delimit its northern and southern borders that form cliffs in the landscape. Geophysical studies carried out on the Adamawa plateau have shown that Pan African faults have cut the crust down to the mantle (Dorbath et al., 1986; Nnange et al., 2000) and thus have served as natural passage for the magma to reach

the surface (Moreau et al., 1987), probably after the mantle melting through adiabatic decompression process (Nkouandou et al., 2010). The Adamawa uprising could have break up the crust-mantle equilibrium system (Njankouo Ndassa, 2020), leading to the evolution of the subcontinental mantle with the modification of its nature, structure and composition (Nkouandou et al., 2015; Njombie et al., 2018; Njankouo Ndassa, 2020). This evolution is ascertained by previous studies on mantle materials brought to the surface by Mio-Pliocene basaltic lavas flows, which have shown that the nature of subcontinental mantle beneath the Adamawa plateau seems rather complex (Nkouandou et Temdjim, 2011; Nkouandou et al., 2015; Njombie et al., 2018) due to it heterogeneous composition, not yet cleared up. Recent petrological studies (Njombie et al., 2018; Njankouo Ndassa, 2020) suggest that the spinel lherzolites from Youkou (south-east of Ngaoundéré) and from the area north of Ngaoundéré have been affected by late metasomatic enrichment induced by hydrous silicate melts and that they must have experienced refertilization processes driven by the infiltration of carbonatite or carbonated silicate melts.

The present work concerns the recently collected peridotite xenoliths from the Lake Guinnadji and Ngao Djalsoka volcano close to the Dibi locality (35 km south of Ngaoundéré) and focuses on their petrographic and geochemical features in order to allow new insights in the nature of Adamawa mantle and its evolution processes.

2. Geological setting

Lake Guinnadji and Ngao Djalsoka are the volcanic structures close to the Dibi locality, which belong to the Adamawa plateau that is a horst of Pan African basement including 630–620 Ma pre- to syn-D1, 580–600 Ma syn-D2 and 550 Ma post-orogenic granitoids (Toteu et al., 1987, 2001; Toteu, 1990). The basement is also composed of pyroxene-and amphibole-bearing gneiss located in the south of Meiganga, showing the geochemical characteristics of Archean TTG (tonalite - trondhjemite - granodiorite), dated of Late Archean (2.6 Ga) to Paleoproterozoic (1.7 Ga) ages by $^{207}\text{Pb}/^{206}\text{Pb}$ single-zircon evaporation method (Ganwa et al., 2008). The recent volcanic episode of Adamawa plateau, dated at 0.91 ± 0.06 Ma, yielded maars and scoria cones with associated basaltic lava flows (Temdjim et al., 2004a), mainly around Ngaoundéré. At the center of Ngaoundéré area, Adamawa basement is covered by basaltic and felsic volcanic lavas of Mio-Pliocene age of 7 to 11 Ma (Gouhier et al., 1974; Temdjim et al., 2004a; Nkouandou et al., 2008). At In the Dibi locality, hillocks of dome shape are composed exclusively of pyroclastite projections which freshness should witness of the most recent volcanic ages. The studied peridotite xenoliths have been sampled in

pyroclastite projections of Dibi. Petrography and mineralogical studies carried out on the Dibi lherzolite peridotites (Girod et al., 1984) sampled from the mantle by pyroclastite projections on their way to the surface have shown that the Moho discontinuity is located at a depth of 20 km, after the whole Adamawa uplift at Tertiary times.

3. Analytical methods

Studied peridotites recently discovered in the pyroclastite projections of Dibi locality have undergone petrographic studies using 10 thin sections prepared at the laboratory GEOPS, University Paris-Saclay, France. Modal proportions of different mineral phases (olivine, orthopyroxene, clinopyroxene, spinel, plus amphibole (?)) of studied peridotite xenoliths selected for this work have been estimated under a polarizing microscope. Major element analyses have been carried out by ICP-OES (Inductively Coupled Plasma - Optical Emission Spectrometry) and trace element analyses by ICP-MS (Inductively Coupled Plasma - Mass Spectrometry) at the Acme Labs of Vancouver, Canada. For the preparation of samples, about 300 mg of powder have been treated with $\text{LiBO}_2/\text{Li}_2\text{B}_4\text{O}$ flux and dissolved in HNO_3 . Crucibles are fused in a furnace. The cooled bead is dissolved in ACS grade nitric acid. Loss on ignition (LOI) was determined by igniting a sample split then measuring the weight loss. For ICP-MS analyses of trace and REE elements, a 0.25g split is heated in $\text{HNO}_3\text{-HClO-HF}$ to fuming and taken to dryness. The residue is dissolved in HCl.

4. Results

4.1. Field work

Studied samples are collected from the pyroclastite deposits around Lake Guinnadji and Ngao Djalsoka volcano (Figure 2A) close to the Dibi locality (Table 1) : both belong to the same volcanic episode aged of 0.91 ± 0.06 Ma (Temdjim et al., 2004b). for sample coordinates Ngao Djalsoka belongs to a ENE trend of volcanic cones (Figure 1C). Of many volcanoes in the area, Ngao Djalsoka is composed of various types of pyroclastite projections including welded tuffs (including blocks of 5-20 cm in size), bombs (10-30 cm in size) and rare blocks 30-60 cm in size, with some showing porous structure, lapilli, volcanic ashes, and in addition some roped lava flows (Figure 2B, C, D). Pyroclastite projections around Lake Guinnadji and Ngao Djalsoka volcano have the same mineral composition: yellowish or bluish olivine crystals, blackish pyroxene crystals and tiny sparkling plagioclase microlites.

Studied peridotite xenoliths have been found in such basaltic blocs (Figure 2). They exhibit yellowish (Figure 2B) or blackish colour (Figure 2C). They are sub-rounded or sub-angular in shape and show sharp **contacts** with basaltic host lava (Figure 2D). The main distinguished minerals of peridotite xenoliths are blue yellowish olivine crystals (60 to 70 volume %) and undistinguished blackish ones (pyroxene, amphibole or spinel?). Whitish crumbly fragments (5 to 7 cm) of crustal origin are packed up in the matrix. The contact between crustal enclave and basaltic host lava show a thin brown corona.

4.2. Petrography

Under **the** plane polarized light (Figure 3), Lake Guinnadji and Djalsoka volcano xenoliths exhibit protogranular (Figure 3A and B) or porphyro**clastic** texture (Figure 3C and D), following the nomenclature of Mercier and Nicolas (1975). All selected samples are mainly composed of olivine, orthopyroxene, clinopyroxene, amphibole (?) and \pm spinel. Large crystals (**olivine, orthopyroxene, clinopyroxene**) are outlined by dots in the borders.

Olivine crystals (4 to 6 mm) are the most abundant component (74-86 %, Table 2). The aggregates of small (< 1mm) recrystallized olivine crystals show mosaic-shaped with straight-lined boundaries. **A few** (2-8 %) clinopyroxene crystals (1 to 2 mm) occur in all samples **especially** in contact with **the** remnant orthopyroxene crystals. Orthopyroxene crystals (10-17 %) are 2 to 4 **mm-large**. Large orthopyroxene crystals (**4 mm**) are mostly remnant and closely **linked** to olivine crystals. All **the** samples **show recrystallization signs marked** are **characterized** by the occurrence of two kinds of olivine and enstatite crystals: large (**6 mm**) elongated and undulated grains (Figures 3A and D) and small (**0.5-1 mm**) generally polygonal strain ones (Figures 3B and C) **that might witness recrystallizations**. Spinel (1-2 %) **is** up to 1 mm in size. **It always shows** vermicular shape and frequently **occurs** between pyroxene crystals. **Some spinels show dot shape feature** Scarce amphibole (?) (2 to 3 mm in size, 0-1 %) crystals occur in some samples (Figure 3A). They are ovoid in shape **and** show small dots in their borders. Estimated volume percentages of mineral phases (Table 2), plot in the field of harzburgite in **the Ol-Opx-Cpx** ternary diagram (Figure 4) of Le Maitre (2002),

4.3. Geochemical studies

Geochemical composition of **some** xenoliths from **the vicinity** of Lake Guinnadji and Djalsoka volcano **is** listed in Table 3. Major elements contents show variable values. SiO₂ **is** between 40.59 and 43.60 wt.%. TiO₂ contents are relatively low (< 0.21 wt.%), samples HD1

and HD3 exhibit the lowest TiO₂ values (0.07-0.06 wt.%). Al₂O₃ contents witness of two groups, low contents (0.62-0.71 wt.% for samples HD1, HD3, HD5 and MO-03) and relatively high contents (1.23-1.54 wt.% for samples HD2, MO-10 and MO-12). Note that CaO contents vary in the same way as Al₂O₃. The highest amounts of Al₂O₃ and CaO correspond to the highest amounts of modal clinopyroxene (5-8 against 2-5 vol.% in the other group, see Table 2). These variations lead to relatively constant CaO/Al₂O₃ ratios for all samples between 0.68 and 0.97, with the mean value close to the Primitive upper mantle value of 0.80 (McDonough and Sun, 1995). Al₂O₃/TiO₂ ratio varies between 4.47 and 11.00.

Total Fe as Fe₂O₃ contents are relatively constant (10.6-15.2 wt.%). MnO contents are low and constant (0.14-0.17 wt.%). MgO contents are high with some variations, leading to contrasting Mg# ($=100 * (\text{MgO}/40.304) / ((\text{MgO}/40.304) + (\text{FeO}/71.844))$) between 85.0 and 88.8.

Alkali contents Na₂O (0.08-0.26 wt.%) and K₂O (0.05-0.13 wt.%) are low for both Lake Guinnadji and Djalsoka volcano. Na₂O/Al₂O₃ ratio ranges between 0.13 and 0.27, compared to 0.11 value of subcontinental mantle (McDonough, 1990). P₂O₅ contents are low (0.03-0.07 wt.%).

SiO₂, Al₂O₃, CaO, Na₂O and TiO₂ contents of studied xenoliths have been plotted against their MgO content (Figure 5). All Harker diagrams show rather negative trends with increasing MgO values.

CIPW normative analyses (Table 3) confirm petrographical observations. Normative olivine (65.7-81.8 wt.%) constitutes the major mineral phase. is strongly dominant Normative hypersthene (9.4-21.2 wt.%) is more abundant than normative diopside (0.2-3.1 wt.%), that is typical of harzburgites.

First transitional elements (Sc, V, Ni, Co and Cr) contents of analysed samples vary widely (see Table 3). Sc contents (7-9 ppm) are low, Ni (2111-2356 ppm), Cr₂O₃ (0.03-0.31 wt.%) and Co (119-169 ppm) contents are high, while V varies between 15-and 53 ppm. Incompatible trace elements contents are low and show wide variation: Rb: 0.8-4.3 ppm, Sr: 14.5-85.5 ppm, Ba: 8-60 ppm, Cs: 0.01-0.1 ppm and Th: 0.1-0.74 ppm. Zr: 5.6-29 ppm and Hf: 0.1-0.6 ppm, giving relatively constant Zr/Hf ratio of 36-56. Nb and Ta contents are also low and give contrasting Nb/Ta ratio (4.3-41) while Nb/Th ratio (8-16) is fairly high. Y (0.6-2.6 ppm) and Ho (0.02-0.1 ppm) gives Y/Ho ratio of 20-40. Sr/Nd ratio of studied peridotites (11.1-15.8) is close to mantle peridotite (Jochum et al., 1989).

Normalized REE ratios of studied xenoliths are shown in Figure 6A. Samples display large variations in REE distribution patterns. Overall, the xenoliths are strongly enriched in

LREE (LaN/SmN = 3.2-13.5). Moreover, LaN/YbN ratio ranges between 11.42 and 23.25. Normalized La is up to 10 times the mantle value, especially for samples of the MO group (Djalsoka volcano) which are characterized by relatively high REE values compared to samples of the HD group (Lake Guinnadji) (Table 3 and Figure 6A).

In primitive mantle-normalized spider diagram (Figure 6B), normalized trace elements display rather regular decrease in values from U to Lu. Samples of MO group are characterized by negative anomalies in K, Ti and also in P. Compared with the samples of MO group, HD group samples display negative anomalies in Ta and positive anomalies in Cs except HD5. All samples exhibit positive anomalies in Zr and most of them for U, except MO-10 and MO-12.

5. Discussion

Geophysical studies carried out on the Adamawa plateau (Dorbath et al., 1986; Poudjom Djomani et al., 1992, 1995; Nnange et al., 2000, 2001) have evidenced the reworking of Pan African faults which have crosscut the Adamawa basement and reach the underlined lithospheric mantle, serving as pathways for the ascending magmas (Moreau et al., 1987). The studied xenoliths might have been sampled in such conditions, probably during transpressional movements of those faults or after upwelling. It has previously been shown, from lherzolite xenoliths equilibria, that the Moho discontinuity is shallow, 20 km beneath the Dibi locality (Girod et al., 1984; Dautria and Girod, 1986) due to the whole Adamawa uplift after the reworking of Pan African faults (Moreau et al., 1987), leading to the compositional evolution of Adamawa subcontinental mantle (Njankouo Ndassa, 2020).

Petrographic and geochemical features of peridotite xenoliths sampled around the Lake Guinnadji and Ngao Djalsoka volcano witness of the complex nature of subcontinental mantle beneath the Dibi volcanic area. Field work data show that peridotite xenoliths occur mainly in the pyroclastite projections exhibiting porous structure. Their sub-rounded or sub-angular shape may reflect the different sample depths within the mantle. Modal and normative analyses (Tables 2 and 3) point out far higher amount of orthopyroxene vs than that of clinopyroxene, which is typical of harzburgite type.

Geochemical data show some variation ranges of major and trace elements (Table 3, Figure 5), which are certainly linked to the compositional diversity of the underlined mantle or processes. ~~because of its evolution It is clear that~~ Geochemical compositions of studied harzburgite xenoliths characterize clearly that materials originated from a depleted mantle. MgO contents (42.4- 45.0 wt.% for Mg# (85.0-88.8) are close to typical harzburgite mantle

(45-47 wt.% MgO for Mg# > 85, Maaløe and Aoki, 1977; McDonough, 1990). As a comparison, Youkou lherzolite presents a higher Mg# ratio of 90.0 for a lower MgO content of 40.0 wt.% (Table 3).

Studied xenoliths exhibit protogranular and porphyroclastic textures which are diagnostic for the mantle peridotites (Mercier and Nicolas, 1975). Remnants and recrystallized features of crystal phases may be interpreted as tectonic markers of their evolutionary setting.

Low contents of incompatible elements and their ratios (Zr/Hf, Nb/Ta, Y/Ho, Sc/Nd) are arguments in favor of mantle materials origin (McDonough and Sun, 1995) of Lake Guinnadji and Ngao Djalsoka volcano peridotites instead of upper mantle fractional crystallization cumulates. The cumulate origin of studied xenoliths is excluded if one considers the fact that all xenoliths exhibit an overall depletion in the HREE, resulting in higher LaN/YbN ratio (11.5-23.3) similar to those of fertile peridotite xenoliths worldwide (McDonough, 1990).

K₂O vs MgO diagram (Figure 7) is used to discriminate xenoliths of cumulate origin from those of off-craton or cratonic origins (after Downes et al., 2004; see discussions in Lee et al., 2000; Downes, 2001). It is clear according to this diagram that The studied xenoliths are clearly residual peridotites of off-craton origin. According to La vs Yb diagram (Figure 8), almost all xenolith samples fall almost within the field of subcontinental harzburgite composition.

The studied xenoliths exhibit low values of CaO/MgO ratio (0.01-0.03), close to those of residual harzburgite peridotites (CaO/MgO < 0.02; Lenoir et al., 2001) and relatively high MgO contents (42.4-45.0 wt.%) compared to samples which have not experienced extensive loss of a basaltic component with ≤ 40.5-41.0 wt.% MgO (Maaløe and Aoki, 1977; McDonough and Sun, 1995). REE data with strong LREE enrichment and LREE/HREE fractionation of the bulk rocks distinguish the Lake Guinnadji and Ngao Djalsoka peridotites as metasomatized harzburgites, as proposed by Downes (2001) for the ultramafic xenoliths from Western and Central Europe.

Mg# vs CaO (wt.%) diagram (Figure 9) and very high LaN/YbN ratio shows that the Lake Guinnadji and Ngao Djalsoka peridotites have experienced a rather high partial melting degree, between 20 and 30 % (Figure 9), and were modified by secondary enrichment process (McDonough and Sun, 1995). It is also worth mentioning that The contrasting geochemical signatures of the whole rock of the studied peridotites (Figure 5) cannot be attributed to melt depletion or only partial melting processes. Rather, the observed enrichments of LREE and

incompatible elements strongly reflect the effect of subsequent metasomatism of the Lake Guinnadji and Ngao Djalsoka volcano peridotites (Meshesha et al., 2014). The occurrence of hydrous phase (amphibole?), suggested in the studied xenoliths, is known in upper mantle (Dawson and Smith, 1982). Spider diagrams (Figure 6) show variable enrichment of incompatible elements especially positive anomalies in U and negative anomalies in Ta leading to variable degrees of cryptic metasomatism (Meshesha et al., 2014). Subcontinental mantle under the Dibi locality might have evolved through two mantle processes: (1) varying degrees of depletion of a fertile mantle by extraction of basaltic melts, leaving a refractory residue, as shown by the systematic negative trends of CaO, SiO₂, Al₂O₃, TiO₂ and Na₂O and (2) modal metasomatism superimposed of the cryptic type. Silicate fluids induce the cryptic type metasomatism, according to relatively higher ratios of Na₂O/Al₂O₃ (0.13-0.27) more than the 0.11 value of primitive mantle (McDonough, 1990), relatively to carbonate type as CaO/Al₂O₃ ratio of analysed samples is close to primitive mantle values (0.80). Moreover, high Zr/Hf (=36-56) and Nb/Ta (=4.3-225.7), which vary wildly relatively to mantle values (Zr/Hf=36.30 and Nb/Ta= 17.5, Sun and McDonough, 1989), are interpreted as the result of pervasive silica melt-solid interaction with significant amounts of trapped melt. The MO-03 sample with low Nb/Ta (4.3) might have interacted with a limited amount of trapped melt (Niu, 2004).

Conclusion

Petrographic and geochemical preliminary data on the protogranular and porphyroclastic textured peridotite xenoliths from the Lake Guinnadji and Ngao Djalsoka volcano point their mantle origin. Rock-forming minerals are essentially olivine and orthopyroxene, and minor amount of clinopyroxene, spinel, plus amphibole (?). Studied xenoliths are harzburgite-type peridotites that have undergone high-degree partial melting, between 20 and 30 %, and have been modified by secondary enrichment processes. The subcontinental mantle under the Dibi locality has evolved through varying degrees of depletion of a more fertile mantle by extraction of basaltic melts and modal metasomatism superimposed on the cryptic-type.

References

Balashov Y.A., 2009. Development of a heterogeneity in the lithosphere: Geochemical evidence. *Petrology* 17, 1, 90-100.

- Dautria, J.M., Girod, M., 1986. Les enclaves de lherzolite à spinelle et plagioclase du volcan de Dibi (Adamaoua, Cameroun): des témoins d'un manteau supérieur anormal. *Bulletin de Minéralogie* 109, 3, 275-286.
- Dawson J.B., Smith J.V., 1982. Upper-mantle amphiboles: a review. *Mineralogical Magazine* 45, 35-46.
- Déruelle B., Ngounouno, I. Demaiffe D., 2007. The 'Cameroon Hot Line' (CHL): A unique example of active alkaline intraplate structure in both oceanic and continental lithospheres. *Comptes Rendus Géoscience* 339, 9, 589-600.
- Dorbath C., Dorbath L., Fairhead J.D., Stuart G.W., 1986. A teleseismic delay time study across the Central African Shear Zone in the Adamawa region of Cameroon, West Africa. *Geophysical Journal of the Royal Astronomical Society* 86, 751-766.
- Downes H0, 2001. Formation and modification of the shallow sub-continental lithospheric mantle: a review of geochemical evidence from ultramafic xenolith suites and tectonically emplaced ultramafic massifs of western and central Europe. *Journal of Petrology* 42, 1, 233-250.
- Downes H., Macdonald R., Upton B.G.J., Cox K.G., Bodinier J.L, Mason, P.R.D., James D., Hill P.G, Hearn Jr C., 2004. Ultramafic xenoliths from the Bearpaw Mountains, Montana, USA: Evidence for multiple metasomatic events in the lithospheric mantle beneath the Wyoming Craton. *Journal of Petrology* 45, 8, 1631-1662.
- Friedman E., Polat A., Thorkelson D.J., Frei, R., 2016. Lithospheric mantle xenoliths sampled by melts from upwelling asthenosphere: The Quaternary Tasse alkaline basalts of southeastern British Columbia, Canada. *Gondwana Research* 33, 209-230.
- Ganwa A.A., Frisch W., Siebel W., Ekodeck G.E., Cosmas S.K., Ngako V., 2008. Archean inheritances in the pyroxene-amphibole bearing gneiss of the Méiganga area (Central North Cameroon): Geochemical and $^{207}\text{Pb}/^{206}\text{Pb}$ age imprints. *Comptes Rendus Géoscience* 340, 211-222.
- Girod M., Dautria J.M., Ball E., Soba D. 1984. Estimation de la profondeur du Moho, sous le massif volcanique de l'Adamaoua (Cameroun), à partir de l'étude d'enclaves de lherzolite. *Comptes Rendus de l'Académie des Sciences, Paris* 298, II,16, 699-704.
- Gouhier J., Nougier J., Nougier D., 1974. Contribution à l'étude volcanologique du Cameroun ('Ligne du Cameroun', Adamaoua), *Annales de la Faculté des Sciences de l'Université de Yaoundé, Cameroun* 17, 3-48.
- Hofmann A.W., 1988. Chemical differentiation of the Earth: The relationship between mantle, continental crust, and oceanic crust. *Earth and Planetary Science Letters* 90,

297-314.

- Ishii T., Robinson P.T., Maekawa H., Fiske R., 1992. Petrological studies of peridotites from diapiric serpentinite seamounts in the Izu-Ogasawara-Mariana Forearc, Leg 125. Proceeding of the Ocean Drilling Program, Scientific Results 125, 445-485.
- Jochum K.P., McDonough W.F., Palme H., Spettel B., 1989. Compositional constraints on the continental lithospheric mantle from trace elements in the spinel peridotite xenolith. *Nature* 340, 548-550.
- Kampunzu A.B., Popoff M., 1991. Distribution of the main Phanerozoic African rifts and associated magmatism: introductory notes. In: Kampunzu A.B. and Lubala R.T. (Eds.) *Magmatism in extensional structural settings. The Phanerozoic African plate.* Springer Verlag, Berlin, pp 2-10.
- Lee C.T., Rudnick R.L., McDonough W.F., Horn I., 2000. Petrologic and geochemical investigation of carbonates in peridotite xenoliths from northeastern Tanzania. *Contributions to Mineralogy and Petrology* 139, 470-484.
- Le Maitre R.W. (Ed.), 2002. *Igneous Rocks, A Classification and Glossary of Terms.* (Recommendations of the IUGS Subcommittee on the Systematics of Igneous Rocks). Cambridge University Press, Cambridge, 252 p.
- Lenoir X., Garrido C.G., Bodinier J.L., Dautria J.M., Gervilla F., 2001. The recrystallization front of the Ronda peridotite: Evidence for melting and thermal erosion of subcontinental lithospheric mantle beneath the Alboran Basin. *Journal of Petrology* 42, 141-158.
- Maaløe S., Aoki K., 1977. The major element composition of the upper mantle estimated from the composition of lherzolites, *Contributions to Mineralogy and Petrology* 63, 161-173.
- McDonough W. F., Sun S.S., 1995. *The Composition of the Earth*, *Chemical Geology* 120, 223-253.
- McDonough W.F., 1990. Constraints on the composition of the continental lithospheric mantle. *Earth and Planetary Science Letters*, 101, 1-18.
- Mercier J.C.C., Nicolas A., 1975. Textures and fabrics of upper-mantle peridotites as illustrated by xenoliths from basalts. *Journal of Petrology* 16, 2, 454-487.
- Meshesha D., Shinjo R., Orihashi Y., 2014. Geochemical and Sr–Nd–Pb isotopic compositions of lithospheric mantle: Spinel lherzolites in alkaline basalts from the northwestern Ethiopian plateau. *Journal of Mineralogical and Petrological Sciences* 109, 241-257.

- Moreau C., Regnault J.M., Déruelle B., Bobineau B., 1987. A new tectonic model for Cameroon line, central Africa. *Tectonophysics* 139, 317-334.
- Niu Y., 2004. Bulk-rock major and trace element compositions of abyssal peridotites: Implications for mantle melting, melt extraction and post-melting processes beneath Mid-Ocean Ridges. *Journal of Petrology* 45, 12, 2423-2458.
- Njankouo Ndassa Z.N., 2020. *Pétrologie et géochimie des péridotites mantelliques en enclaves dans les basaltes au nord de Ngaoundéré: nature du manteau subcontinental du plateau de l'Adamaoua (Plateau de l'Adamaoua, Cameroun, Afrique centrale)*. Thèse de l'Université de Ngaoundéré, Cameroun 232 pp +annexe.
- Njombie M.P.W., Temdjim R., Foley S.F., 2018. Petrology of spinel lherzolite xenoliths from Youkou volcano, Adamawa Massif, Cameroon Volcanic Line: mineralogical and geochemical fingerprints of sub-rift mantle processes. *Contributions to Mineralogy and Petrology* 173, 13.
- Nkouandou O.F., Bardintzeff J.M., Fagny A.M., 2015. Sub-continental lithospheric mantle structure beneath the Adamawa plateau inferred from the petrology of ultramafic xenoliths from Ngaoundéré (Adamawa plateau, Cameroon, Central Africa). *Journal of African Earth Sciences* 111, 26-40.
- Nkouandou O.F., Ngounouno I., Déruelle B., 2010. Géochimie des laves basaltiques récentes des zones Nord et Est de Ngaoundéré (Plateau de l'Adamaoua, Cameroun, Afrique Centrale): pétrogenèse et nature de la source. *International Journal of Biological and Chemical Sciences* 4, 4, 984-1003.
- Nkouandou O.F., Ngounouno I., Déruelle B., Ohnenstetter D., Montigny R., Demaiffe D., 2008. Petrology of the Mio-Pliocene Volcanism to the North and East of Ngaoundéré (Adamawa-Cameroon). *Comptes Rendus Géoscience* 340, 27-38.
- Nkouandou O.F., Temdjim R., 2011. Petrology of spinel lherzolite xenoliths and host basaltic lava from Ngao Voglar volcano, Adamawa Massif (Cameroon Volcanic Line, West Africa): equilibrium conditions and mantle characteristics. *Journal of Geosciences* 56, 375-387.
- Nnange J.M., Ngako V., Fairhead J.D., Ebinger C.J., 2000. Depths to density discontinuities beneath the Adamawa Plateau region, Central Africa, from spectral analyses of new and existing gravity data. *Journal of African Earth Sciences* 30, 4, 887-901.
- Nnange J.M., Poudjom Djomani Y.H., Fairhead J.D., Ebinger C., 2001. Determination of the isostatic compensation mechanism of the region of the Adamawa dome, West Central

- Africa using the admittance technique of gravity data. *African Journal of Science and Technology* 1, 4, 29-35.
- Poudjom Djomani Y.H., Diament M., Albouy Y., 1992. Mechanical behavior of the lithosphere Beneath the Adamawa Up lift (Cameroon, West Africa) based on gravity data. *Journal of African Earth Sciences* 15, 81-90.
- Poudjom Djomani Y.H., Nnange J.M., Diament M., Ebinger C.J., Fairhead J.D., 1995. Effective elastic thickness and crustal thickness variation in west central Africa inferred from gravity data. *Journal of Geophysical Research* 100, 22047-22070.
- Sun, S.-S., McDonough, W.F., 1989. Chemical and isotopic systematics in ocean basalt: implications for mantle composition and processes. In: Saunders, A. D. & Norry, M. J. (Eds.) *Magmatism in the Ocean Basins*. Geological Society, London, Special Publications 42, 313-345.
- Tamen J., Nkoumbou C., Reusser E., Tchoua F., 2015. Petrology and geochemistry of mantle xenoliths from the Kapsiki Plateau (Cameroon Volcanic Line): Implications for lithospheric upwelling. *Journal of African Earth Sciences* 101, 119-134.
- Temdjim, R., Boivin, P., Chazot, G., Robin, C., Rouleau, E., 2004a. L'hétérogénéité du manteau supérieur à l'aplomb du volcan de Nyos (Cameroun) révélée par les enclaves ultrabasiques. *Comptes Rendus Géoscience* 336, 1239-1244.
- Temdjim R., Njilah I.K., Kamgang P., Nkoumbou C., 2004b. Données nouvelles sur les laves felsiques de Ngaoundéré (Adamaoua, ligne du Cameroun): chronologie K-Ar et pétrologie. *African Journal of Science and Technology* 5, 2, 113-123.
- Toteu S.F., 1990. Geochemical characterization of the main petrographical and structural units of Northern Cameroon: implications for Pan-African evolution. *Journal of African Earth Sciences* 10, 4, 615-624.
- Toteu S.F., Michard A., Bertrand J.M., Rocci G., 1987. U/Pb dating of Precambrian rocks from northern Cameroon, orogenic evolution and chronology of the Pan-African belt of Central Africa. *Precambrian Research* 37, 1, 71-87.
- Toteu S.F., Van Schmus W.R., Penaye J., Michard A., 2001. New U-Pb and Sm-Nd data from north-central Cameroon and its bearing on the pre-Pan African history of central Africa. *Precambrian Research* 108, 1-2, 45-73.

Table captions

Table 1. Coordinates of the Lake Guinnadji and Ngao Djalsoka volcano peridotite xenoliths.

Table 2. Modal compositions (in vol.%) of the studied peridotite xenoliths.

Table 3. ICP-MS and ICP-AES analyses of whole rock major and trace elements and REE analyses of the Lake Guinnadji and Ngao Djalsoka volcano harzburgites and their CIPW normative compositions; note that LOI is negative as all Fe is measured as Fe₂O₃. The composition of Youkou lherzolite analysis (Njombie et al., 2018) is added for comparison.

Figure captions

Figure 1. A: Main African cratons, B: Cameroon volcanic line and Adamawa plateau volcanic area (modified after Kampunzu and Popoff, 1991; Déruelle et al., 2007), C: Location of studied area of the Guinnadji Lake and Djalsoka volcano.

Figure 2. A: Panoramic view of the north hillside of Djalsoka volcano, B: Sub-angular, C: Sub-rounded, and D: Rounded shape of studied peridotite xenoliths. Scale indicated by a coin.

Figure 3. Photomicrographs of Lake Guinnadji and Ngao Djalsoka xenolith textures. A and B: Protogranular, C and D: Porphyroclastic textures. Scale bar represents 1 mm. amph = amphibole, cpx = clinopyroxene, opx = orthopyroxene, spl = spinel.

Figure 4. Nomenclature of studied peridotite xenoliths according to the classification scheme of Le Maitre (2002). Dibi (this study): Lake Guinnadji (square) and Ngao Djalsoka volcano (triangle). Data from Youkou, Kapsiki plateau and Ngao Voglar are added for comparison.

Figure 5. Major oxide contents vs MgO content Harker diagrams of the Lake Guinnadji and Ngao Djalsoka volcano xenoliths.

Figure 6. Chondrite-normalized REEs (a) and primitive mantle-normalized trace elements (b) abundances of the studied peridotite xenoliths according to McDonough and Sun (1995).

Figure 7. K₂O vs MgO diagram for studied xenoliths. Lake Guinnadji (square), Ngao Djalsoka volcano (triangle), Youkou (circle). Fields of off-craton and cratonic mantle spinel peridotites from Downes et al. (2004). Compositions outside of these fields correspond to cumulates.

Figure 8. Peridotite xenoliths from Ngao Djalsoka and Lake Guinnadji plotted in La vs Yb diagram after Balashov (2009). Youkou lherzolite (Njombie et al., 2018) is plotted for comparison. BSE = Bulk Silicate Earth “pyrolite”, DM-EM line = Depleted Mantle - Enriched Mantle. Same symbols as in Figure 9.

Figure 9. Mg# vs CaO (wt.%) diagram for Lake Guinnadji and Ngao Djalsoka peridotites. Same symbols as in Figure 8. Added for comparison: Youkou lherzolite (circle, Njombie et al., 2018), Torishima and Conical Seamount: the dark gray shaded area corresponds to harzburgite, data and the light grey shaded area to dunite (from Ishii et al., 1992). Percentages of partial melting from a primitive source are indicated by the line at the top (from Friedman et al., 2016).

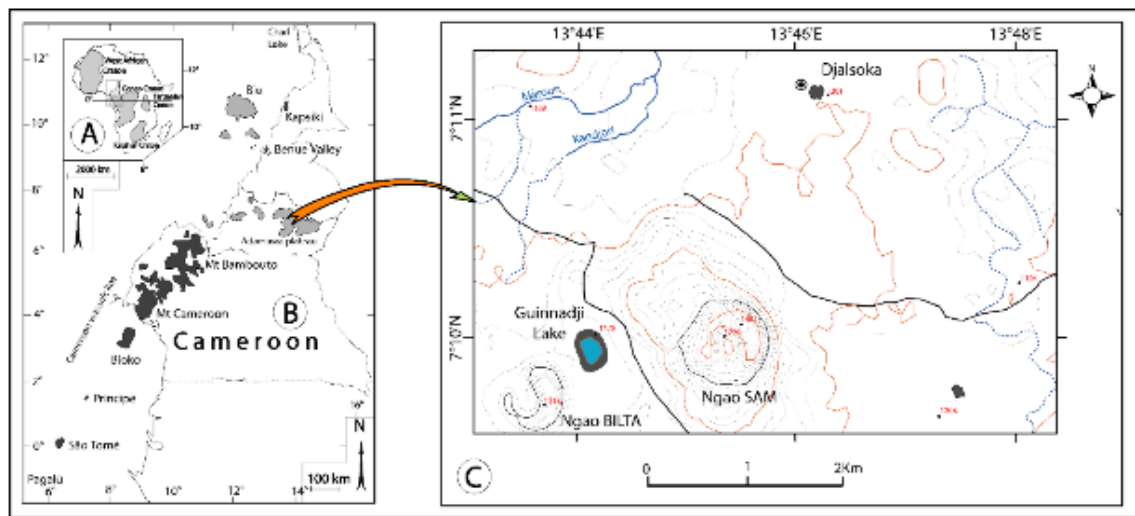


Figure 1

UNDER REVIEW

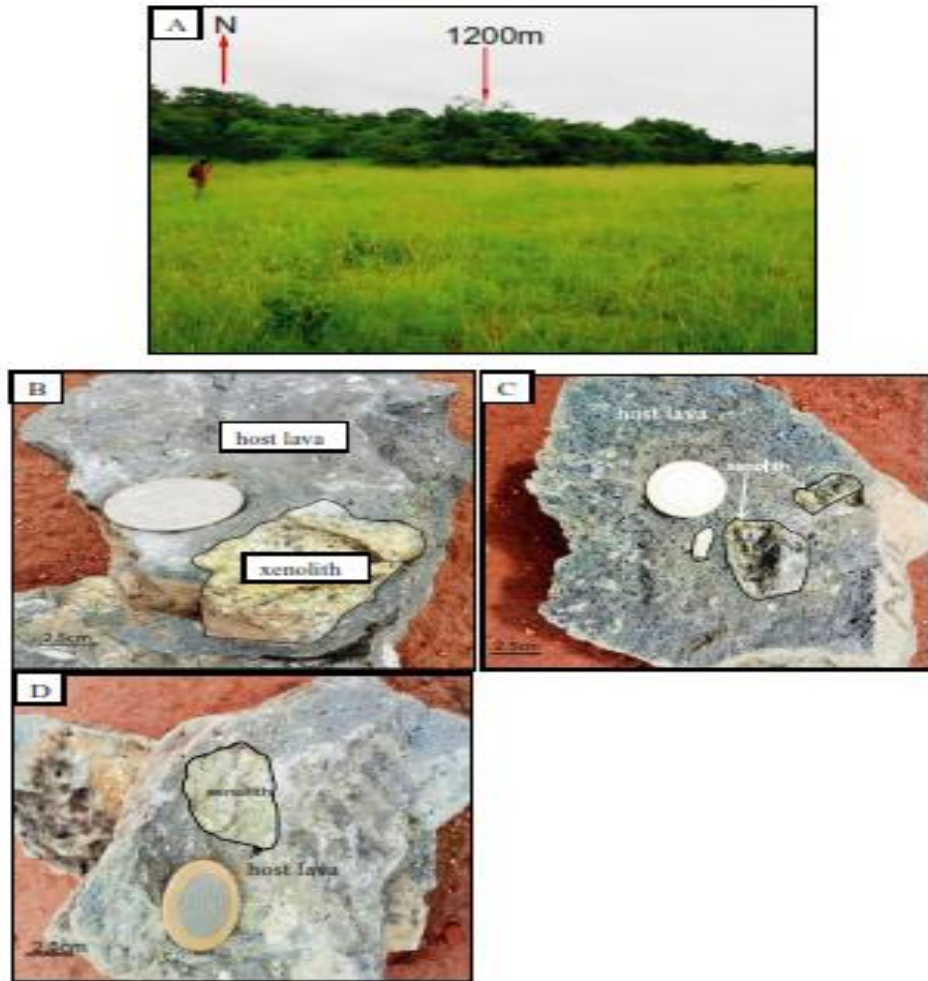


Figure 2

UNDER REVIEW

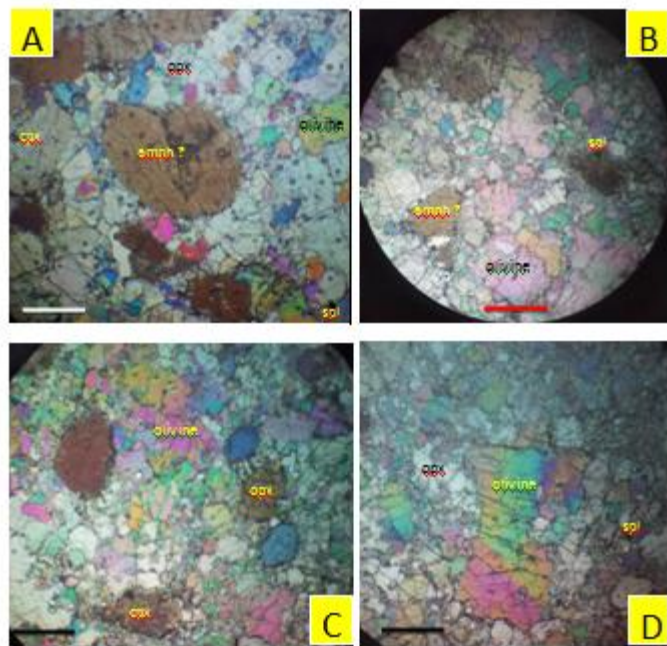


Fig 3

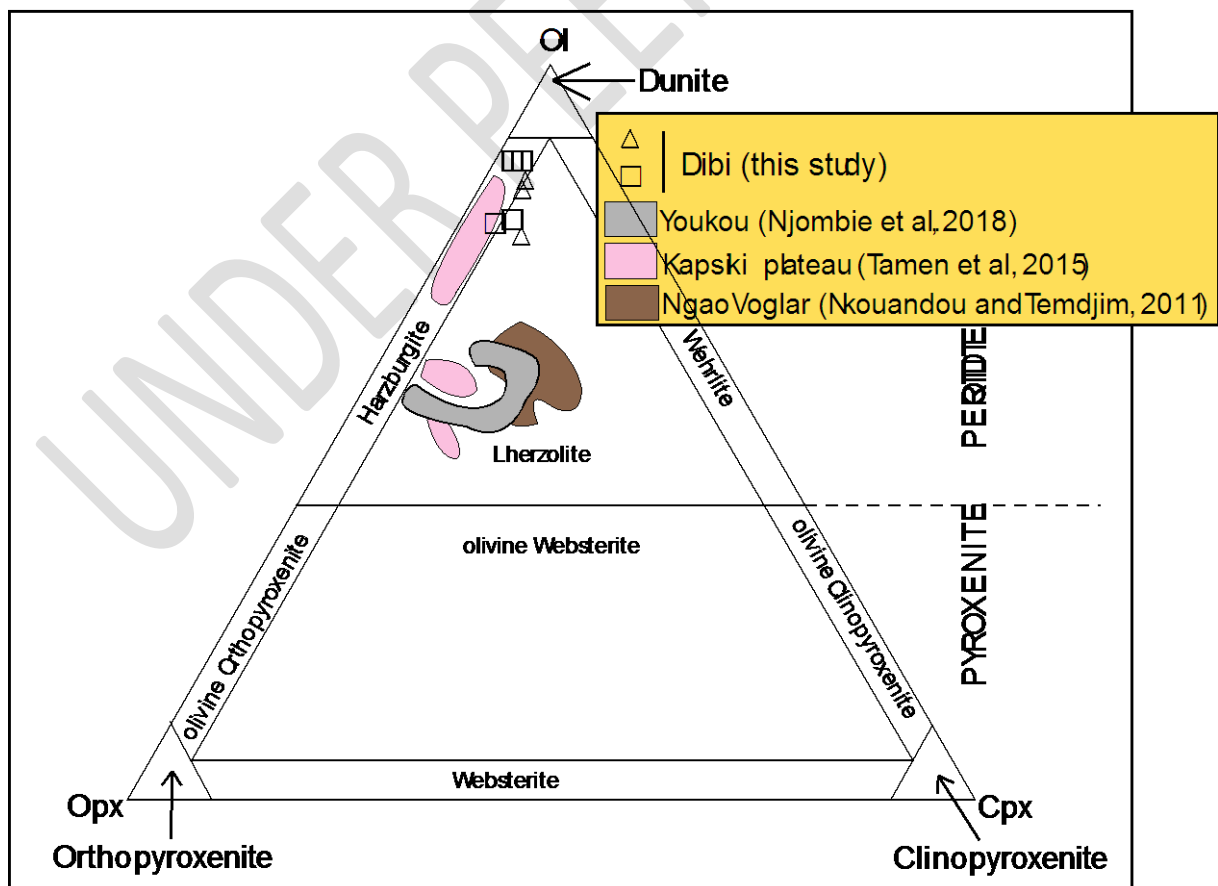


Fig 4

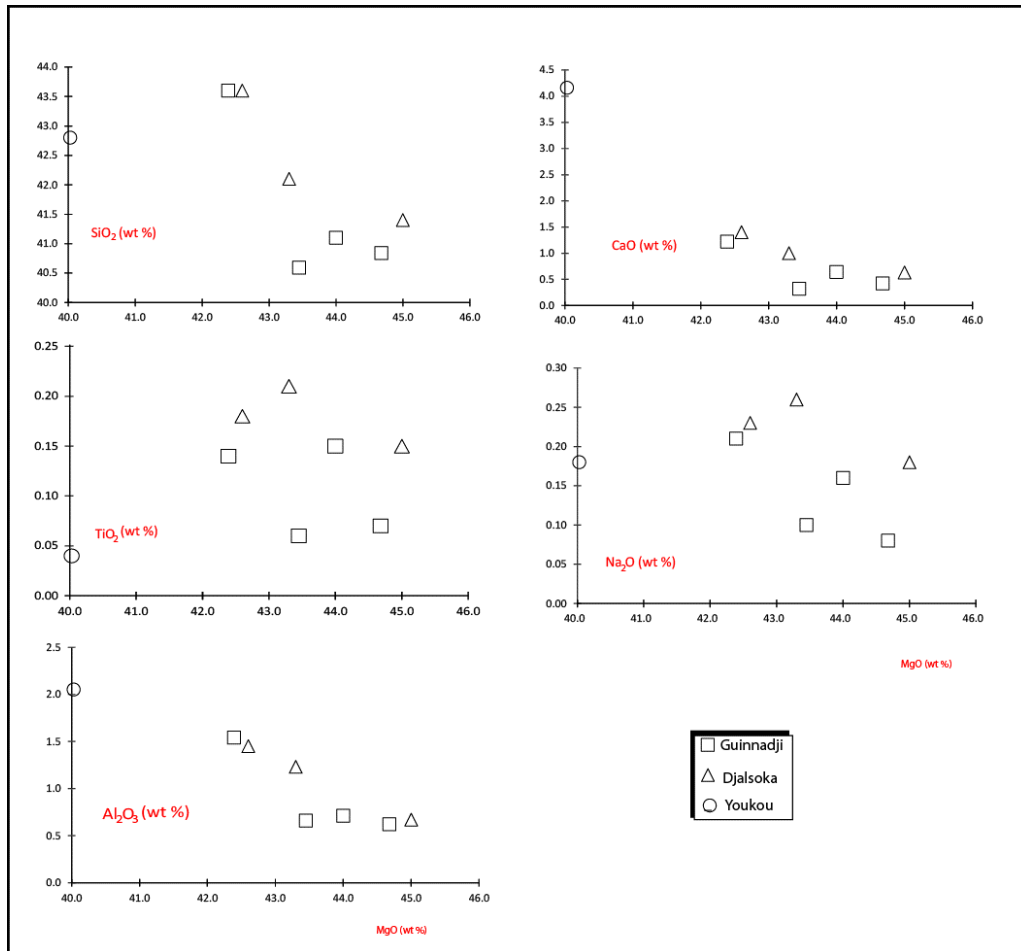


Fig 5

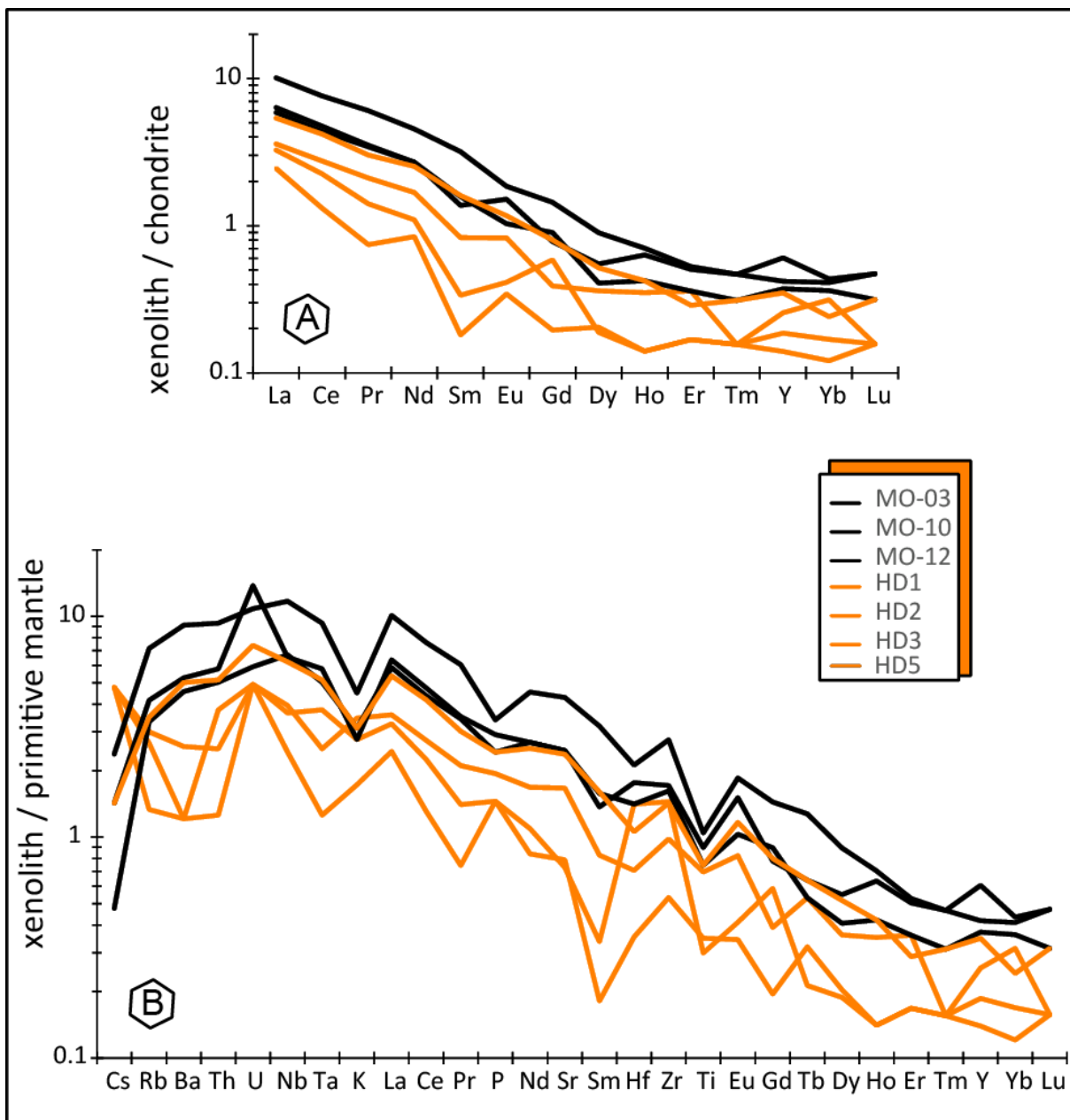


Fig 6

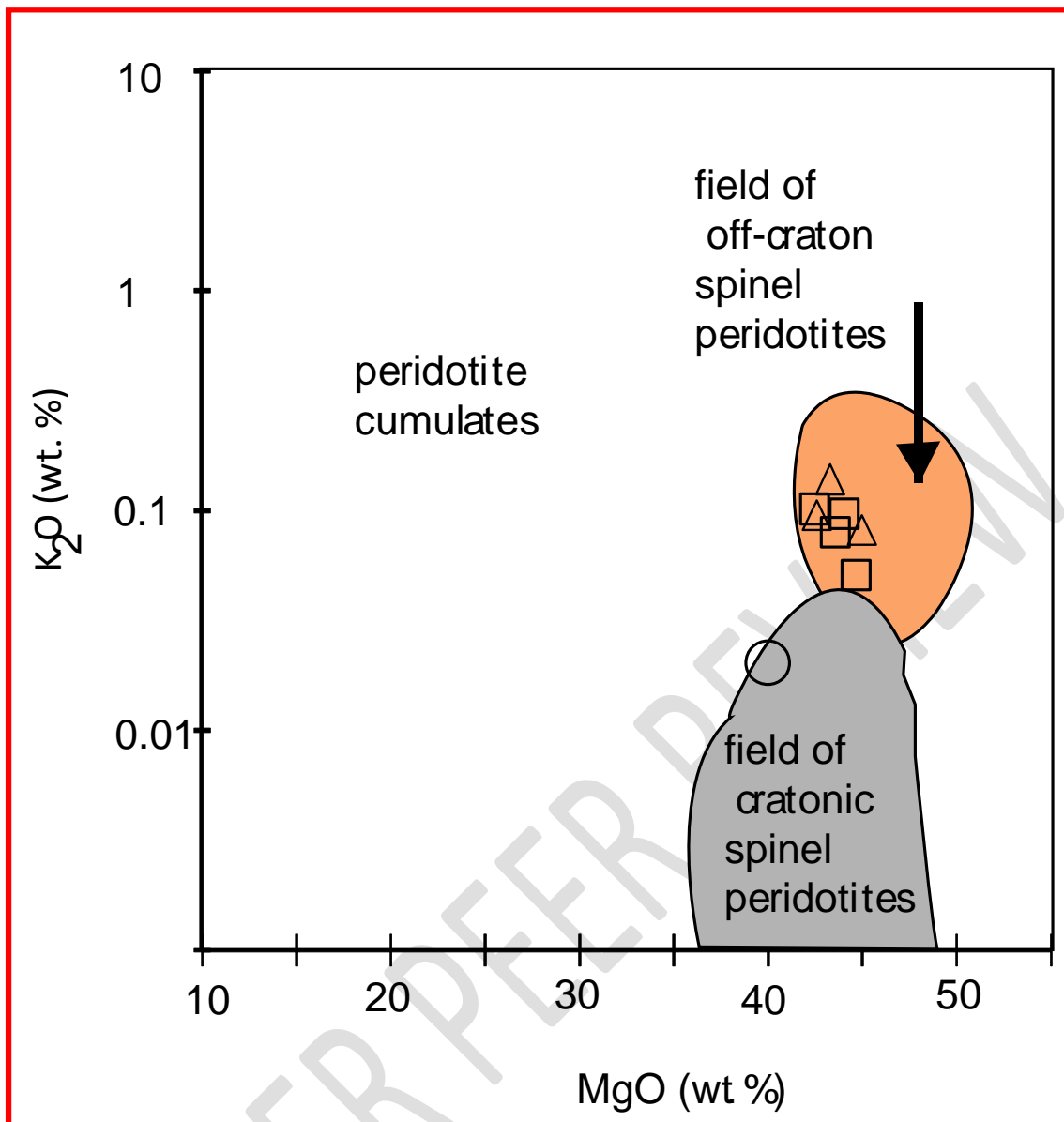


Fig 7

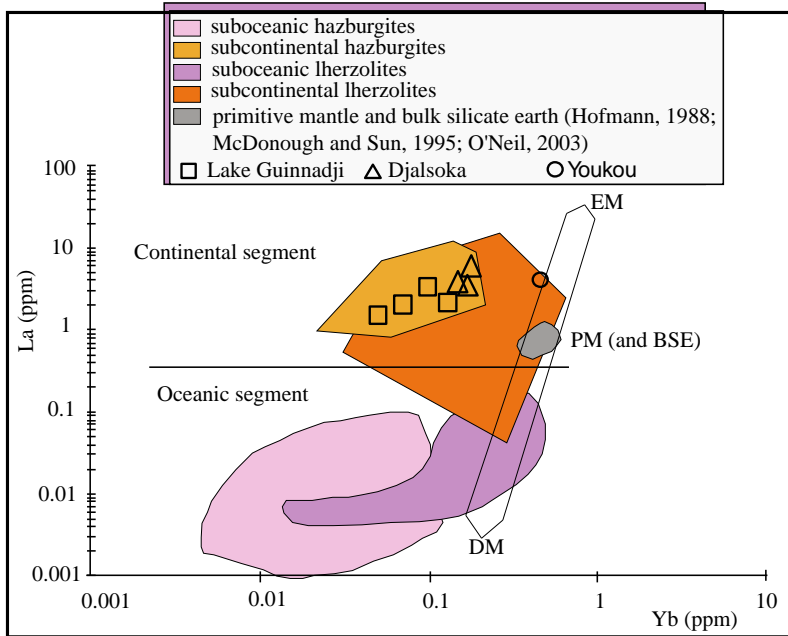


Fig 8

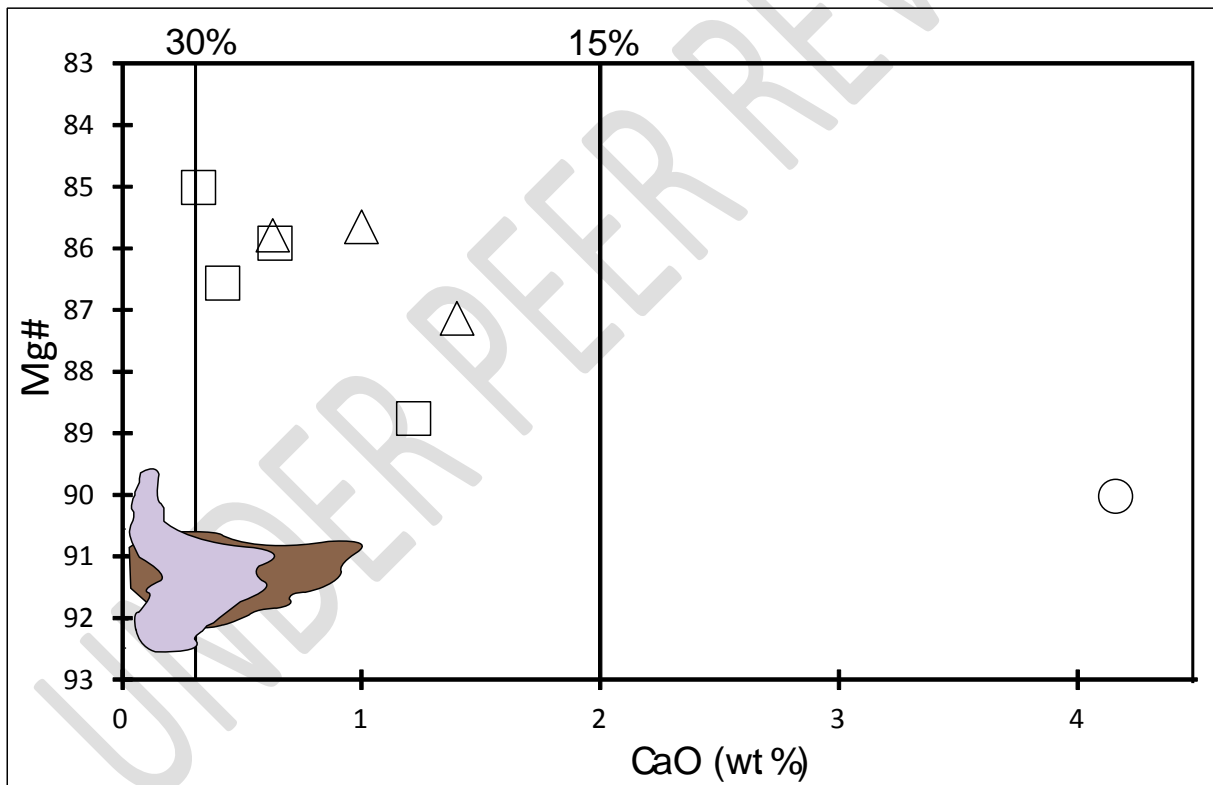


Fig 9

Table 1.

Site	Sample	Coordinate
------	--------	------------

Locality	Sample	Olivine	Orthopyroxene	Clinopyroxene	Spinel	Amphibole
Guinnadji	HD1	85	10	3	1	1
Guinnadji	HD2	78	15	6	1	0
Guinnadji	HD3	86	11	2	1	0
Guinnadji	HD5	76	17	4	2	1
Djalsoka	MO-03	82	11	5	1	1
Djalsoka	MO-10	74	15	8	2	1
Djalsoka	MO-12	81	12	5	1	1

Lake Guinnadji	HD1	N07°09'35'' E13°44'32''
Lake Guinnadji	HD2	N07°09'34'' E13°44'34''
Lake Guinnadji	HD3	N07°09'33'' E13°44'35''
Lake Guinnadji	HD5	N07°09'30'' E13°44'33''
Djalsoka volcano	MO-12	N07°10'35'' E13°45'06''
Djalsoka volcano	MO-03	N07°10'45'' E13°45'23''
Djalsoka volcano	MO-10	N07°10'45'' E13°45'29''

Table 2.

Table 3 :

Locality	Guinnadji	Guinnadji	Guinnadji	Guinnadji	Djalsoka	Djalsoka	Djalsoka	Youkou
Sample	HD1	HD2	HD3	HD5	MO-03	MO-10	MO-12	N-35
Rock	harzburgi te	harzburgi te	harzburgi te	harzburgi te	harzburgi te	harzburgi te	harzburgi te	lherzoli te
SiO ₂ (wt %)	40.84	43.60	40.59	41.10	41.40	42.10	43.60	42.81
TiO ₂	0.07	0.14	0.06	0.15	0.15	0.21	0.18	0.04

Al ₂ O ₃	0.62	1.54	0.66	0.71	0.67	1.23	1.45	2.05
Fe ₂ O ₃	13.76	10.62	15.16	14.25	14.75	14.40	12.45	8.74
MnO	0.15	0.14	0.17	0.16	0.16	0.16	0.15	0.17
MgO	44.68	42.39	43.45	44.00	45.00	43.30	42.60	40.03
CaO	0.42	1.22	0.32	0.64	0.63	1.00	1.40	4.16
Na ₂ O	0.08	0.21	0.10	0.16	0.18	0.26	0.23	0.18
K ₂ O	0.05	0.10	0.08	0.09	0.08	0.13	0.09	0.02
P ₂ O ₅	0.03	0.04	0.03	0.05	0.06	0.07	0.05	0.86
LOI	-1.10	-0.70	-1.00	-1.16	-1.21	-1.18	-1.00	0.23
sum	99.60	99.30	99.62	100.15	101.87	101.68	101.20	99.29
Mg#	86.57	88.77	85.02	85.92	85.79	85.65	87.14	90.03
CIPW								
norm								
Plagioclase	1.89	4.77	1.99	2.33	2.33	4.03	4.63	6.28
Orthoclase	0.30	0.59	0.47	0.53	0.47	0.77	0.53	0.12
Diopside	0.53	2.24	0.20	1.51	1.55	2.14	3.13	8.08
Hypersthene	12.09	21.21	13.25	11.35	9.40	11.94	18.54	16.32
Olivine	79.04	65.70	77.19	78.30	81.78	76.45	68.89	61.96
Ilmenite	0.13	0.27	0.11	0.28	0.28	0.40	0.34	0.08
Magnetite	6.64	5.12	7.32	6.89	7.12	6.96	6.00	4.20
Apatite	0.07	0.09	0.07	0.12	0.14	0.16	0.12	2.02
Be (ppm)	1	1	1					
Rb	0.8	1.8	1.6	2.1	2.5	4.3	2	
Sr	15.7	33.2	14.5	47.3	49.1	85.5	49.1	105
Cs	0.1	0.1	0.1	0.03	0.03	0.05	0.01	14.9
Ba	8	17	8	33.1	34.8	60.2	30.1	24
V	15	38	16	16	15	28	53	52
Cr ₂ O ₃ (wt %)	0.057	0.313	0.028	0.042	0.032	0.071	0.177	0.2643
Co	146.7	119.2	168.9					114
Ni	2356	2309	2111					2408
Y	0.6	1.1	0.8	1.5	1.6	2.6	1.8	3
Zr	5.6	10.3	15.2	15	17	29	18	16
Hf	0.1	0.2	0.4	0.3	0.4	0.6	0.5	0.076
Nb	1.6	2.6	2.4	4.1	4.3	7.7	4.4	0.48
Ta	0.1	0.2	0.1	0.1	1	0.3	0.3	0.182
Th	0.1	0.2	0.3	0.41	0.46	0.74	0.4	0.27
U	0.1	0.1	0.1	0.15	0.28	0.22	0.12	0.101
La	1.5	2.2	2	3.3	3.9	6.2	3.6	2.46
Ce	2.1	4.4	3.6	6.7	7.6	12.2	7	4.85
Pr	0.18	0.51	0.34	0.73	0.85	1.46	0.83	0.45
Nd	1	2	1.3	3	3.2	5.4	3.2	1.51
Sm	0.07	0.32	0.13	0.62	0.61	1.23	0.53	0.193
Eu	0.05	0.12	0.06	0.17	0.15	0.27	0.22	0.083
Gd	0.2	0.26	0.15	0.35	0.54	0.93	0.42	0.29

Tb	0.03	0.05	0.02	0.06	0.05	0.12	0.06	
Dy	0.13	0.23	0.12	0.33	0.26	0.57	0.35	0.35
Ho	0.02	0.05	0.02	0.06	0.06	0.1	0.09	0.086
Er	0.07	0.15	0.07	0.12	0.15	0.22	0.21	0.24
Tm	0.01	0.01	0.01	0.02	0.02	0.03	0.03	
Yb	0.05	0.13	0.07	0.1	0.15	0.18	0.17	0.24
Lu	0.01	0.01	0.01	0.02	0.02	0.03	0.03	0.046
Ga	0.7	1.8	0.9	1.5	1.5	2.8	2.7	1
Sn	1	1	1	<1	<1	<1	<1	
Sc	7	9	7					14.9
W	0.5	0.5	0.6	<1	<1	<1	1	
Al ₂ O ₃ /MgO	0.01	0.04	0.02	0.02	0.01	0.03	0.03	0.05
Al ₂ O ₃ /TiO ₂	8.86	11.00	11.00	4.73	4.47	5.86	8.06	51.25
CaO/Al ₂ O ₃	0.68	0.79	0.48	0.90	0.94	0.81	0.97	2.03
CaO/MgO	0.01	0.03	0.01	0.01	0.01	0.02	0.03	0.10
Na ₂ O/Al ₂ O ₃	0.13	0.14	0.15	0.23	0.27	0.21	0.16	0.09
Na ₂ O/TiO ₂	1.14	1.50	1.67	1.07	1.20	1.24	1.28	4.50
Ba/Rb	10.00	9.44	5.00	15.76	13.92	14.00	15.05	
Nb/Ta	16.00	13.00	24.00	41.00	4.30	25.67	14.67	2.64
Nb/Th	16.00	13.00	8.00	10.00	9.35	10.41	11.00	1.78
Sr/Nd	15.07	16.60	11.15	15.77	15.34	15.83	15.34	69.54
Y/Ho	30.00	22.00	40.00	25.00	26.67	26.00	20.00	34.88
Y/Nb	0.38	0.42	0.33	0.37	0.37	0.34	0.41	6.25
Zr/Hf	56.00	51.50	38.00	50.00	42.50	48.33	36.00	210.53
GdN/YbN	1.62	1.24	3.46	3.31	2.48	3.32	1.90	0.91
LaN/SmN	13.49	4.33	9.69	3.35	4.03	3.17	4.28	8.02
LaN/YbN	20.25	11.42	19.29	22.28	17.55	23.25	14.29	6.92
TbN/YbN	2.65	1.70	1.26	2.65	1.47	2.94	1.56	0.00